Closing the UV-Induced Photodegradation Gap Through Global Scale Modeling of Fixed Tilt and Tracking Photovoltaic Systems

S. Poddar, S. Liu, P. Hamer, M. Kay, and B. Hoex

***Abstract*—Ultraviolet (UV) radiation accelerates the degradation of photovoltaic (PV) modules, both at the cell and module levels, leading to reduced efficiency and a shorter lifespan. While reliability testing has advanced, current standards often fail to reflect real-world UV exposure, especially across diverse climates. Global UV irradiance varies widely, from <30 W/m^2 in high-latitude regions to >80 W/m^2 in arid zones, while standard tests such as IEC-61215 only test up to a dose of 15 kWh /m^2 that can be reached in less than 50 days in some locations. This study develops a high-precision model to estimate UV radiation on tilted surfaces and assesses the influence on UV photodegradation. The model shows minimum bias (<±3.87 W/m^2, i.e., <±4.28%) when compared with observations. Results show notable global variation in UV irradiance on tilted surfaces between single-axis tracking (SAT) and fixed-tilt systems, hence affecting degradation rates. SAT systems experience approximately twice the degradation in arid and semi-arid climates compared to fixed-tilt systems, where UV exposure is most intense. These findings highlight the critical need for climate-specific degradation assessments even for identical module technologies. To ensure outdoor durability and long-term performance, advanced regionally adaptive reliability testing thresholds should be adapted for better-informed material selection and manufacturing.**

***Index Terms*—Degradation modeling, fixed tilt, single-axis tracking (SATs), ultraviolet (UV)-irradiance modeling, UV photodegradation.**

I. Introduction

Solar photovoltaic (PV) system deployment and grid integration has surged globally to meet energy demands and net zero targets. In order to meet the target of constraining global warming to 1.5 °C by 2050, renewable energy should account for 91% of total energy consumption, with a growing share of electricity in the energy mix [1]. Among renewables, solar PV is expected to be one of the largest contributors [2]. The lifetime and durability of a PV system directly affect the levelized cost of energy and return on investment. Therefore, to ensure a successful energy transition, it is crucial to thoroughly investigate the various degradation modes affecting the reliability of the PV systems and, in particular, the PV modules. PV modules typically have a performance warranty of 25–30 years [3], guaranteeing at least 80% of the rated power at the end of this period. Apart from an initial power drop of 1% –2% in the first year, the subsequent power decline is expected to occur uniformly throughout the module's remaining lifetime. However, previous studies have reported that the modules degrade at varied rates depending on their location globally [4]. This is due to the influence of regional climate on the modules that can initiate climate-specific degradation modes, such as encapsulant discoloration, corrosion, internal circuit failure, delamination, and light-induced degradation.

There has been extensive research showing that prolonged exposure to ultraviolet (UV) radiation can lead to encapsulant discoloration, delamination, backsheet cracking, and premature aging of the module materials, including degradation of the PV cells due to a decrease in surface passivation [4], [5], [6], [7], [8]. Most of the surface solar radiation falls within the 300–2500 nm wavelength range, encompassing UV light (<380 nm), visible light (380–780 nm), and infrared light (>780 nm). UV light consists of photons with short wavelengths and high energies, typically leading to shallow penetration depths. The amount of surface reaching solar radiation is affected by the presence of atmospheric components, such as clouds, aerosols, atmospheric gases, etc., that can lead to scattering or absorption of solar radiation [9]. Depending on the location, the surface reaching UV radiation can vary significantly due to the presence of ozone, clouds, and other atmospheric components.

It is reported that UV-induced degradation is more common in hot climates [4], [10]. The UV irradiation mainly affects the encapsulant [for example, ethyl-vinyl acetate (EVA)] and semiconductor material. Historically, EVA was preferred for the majority of the modules due to its lower cost, optical properties, and long-term field experience [11]. Exposure of EVA to heat, humidity, and UV radiation can produce acetic acid, which causes the encapsulant to turn yellow or brown. As a result, EVA absorbs more high-energy visible light, particularly in the blue and violet wavelengths, thereby reducing the module's efficiency [12]. This effect can further be intensified by elevated temperatures and result in localized hot spots. The discolored encapsulant reduces light transmission, leading to a reduction in short-circuit current [13] and a drop in power generation [5]. More recent modules utilize newer materials, such as polyolefin

Received 27 September 2025; revised 5 December 2025; accepted 23 February 2026. This work was supported in part by the Australian Government through the Australian Renewable Energy Agency under Grant TRAC 2022/12 and in part by the Australian Centre for Advanced Photovoltaics. *(Corresponding author: S. Poddar.)*

The authors are with the School of Photovoltaic and Renewable Energy Engineering, University of New South Wales, Sydney, NSW 2052, Australia (e-mail: s.poddar@unsw.edu.au).

Digital Object Identifier 10.1109/JPHOTOV.2026.3668778

elastomer-based and thermoplastic polyolefin-based encapsulants, to prevent acetic acid formation. It should also be noted that module architecture plays an important role. In older monofacial glass–backsheet designs, any acetic acid produced could diffuse through the backsheet, whereas in glass–glass modules, this diffusion pathway is significantly restricted.

UV-induced degradation is relatively more pronounced in modern high-efficiency silicon (Si) cells in comparison to the previous generations, while significant efforts have been made to mitigate UV-induced degradation through the incorporation of UV-blocking additives in encapsulants and optimized antireflective coatings. However, recent advances in high-efficiency cell architectures increasingly prioritize enhanced external quantum efficiency. This shift has led to the adoption of features such as higher emitter sheet resistances and more UV-transparent materials, which may inadvertently increase the sensitivity of modern devices to UV exposure. Consequently, cell architectures such as tunnel oxide passivated contact (TOPCon), heterojunction technology (HJT), and passivated emitter rear contact (PERC) have been reported to exhibit increased sensitivity to UV radiation due to their material and optical design [14]. Early silicon heterojunction module designs also demonstrated notable UV-induced degradation, which has been linked to the degradation of Si–H bonds and reduction in hydrogen content within the passivation layers [15], [16]. Recently, the impact of UV-induced degradation was studied for commercial TOPCon modules, and 40% of the tested modules experienced a power loss of more than 5% after exposure to a UV dose of just 60 kWh/m^2 [14]. This level of degradation is notable because a 60 kWh/m^2 UV dose corresponds to roughly one year in moderate climates and even less in high-UV regions, such as Australia. A recent study on bifacial n-type passivated emitter rear totally diffused solar cells reported a 15% power drop after being exposed to 598 kWh/m^2 of UV dose [17]. Furthermore, several studies have revealed that at the cell level, UV-induced degradation plays a key role in breaking covalent bonds such as Si–H bonds in passivating films, which may result in hydrogen accumulation near the passivation interface, ultimately influencing the effectiveness of surface passivation. [17], [18], [19]. The effectiveness of surface passivation relies on semiconductor and dielectric thin films, with Si–H bonds playing a crucial role in maintaining chemical stability and protection. Moreover, this is expected to have a higher impact on the bifacial modules as both front and back are now exposed to UV [20], [21]. Therefore, it is essential to accurately model the UV irradiation on the PV modules to precisely estimate their degradation rates and performance.

UV stress testing is typically conducted in a weathering chamber under accelerated environmental conditions. This approach helps assess module durability in the field by simulating real-world long-term failure mechanisms and modes within a shorter timeframe, usually spanning two to six months [10]. The IEC 61215 standard specifies a UV preconditioning test requiring only 15 kWh/m^2 total UV irradiance dosage in the 280–400 nm wavelength range and a module temperature of 60 ± 5 °C. This dosage is roughly equal to only 46 days of field exposure in Arizona, USA. This dose is insufficient to induce encapsulant discoloration and does not accurately reflect the lifetime UV exposure on modules. For a more realistic testing, the updated quality plus protocol suggests UV stress testing at a higher dosage of 225 kWh/m^2, which is still only equivalent to approximately two years in Arizona [22]. In the past, several statistical and physics-based models have been proposed to estimate the UV degradation rate of the modules in the field [4], [23], [24]. These models consider UV dose, relative humidity on the module surface, module temperature, and activation energy necessary for photoreaction induced degradation. Previous studies have calibrated these models using lab tests and have been found to have minimum bias overall.

Despite these advances in modeling approaches and accelerated testing methods, there remains a significant challenge in how we model UV radiation on tilted surfaces for estimating photodegradation rates. There are limited spectral radiometers across the world that record UV radiation, and all the satellite products only provide ground-reaching UV radiation. In the past, degradation rate modeling studies have used horizontal UV irradiance [4], [25]. The use of UV radiation on horizontal surfaces for estimating UV photodegradation rates on tilted surfaces can lead to inaccurate lifetime predictions.

Globally, the most measured data for solar radiation is on a horizontal surface, due to the simplicity and standardization of horizontal irradiance sensors across most meteorological stations. Accurate PV energy yield estimation relies on robust modeling of plane-of-array (POA) irradiance using transposition models. These models convert horizontal irradiance data into irradiance on tilted PV surfaces by accounting for direct, diffuse, and ground-reflected components. The diffuse component is highly sensitive to sky irradiance distribution. Performance of transposition models varies with climate, regional weather, solar geometry, and system design, and studies show anisotropic models outperform isotropic models when validated against field data [26], [27], [28], [29], [30]. Small errors in tilt or azimuth can introduce measurable biases in annual energy yield. In densely packed PV arrays, row-to-row shading further reduces irradiance by partially blocking both diffuse and circumsolar radiation, resulting in the lower sections of tilted modules receiving significantly less energy. Recent modeling approaches explicitly incorporate view factors and shading of both direct and diffuse components to improve predictions for interior rows [27], [28]. As a result, there have been extensive studies in the past to develop analytical algorithms that convert horizontal irradiance to tilted irradiance for optimizing solar energy generation. The two main primary approaches to model tilted irradiance include isotropic and anisotropic sky models [31], [32], [33]. Both models handle the beam and ground-reflected components similarly, but they differ significantly in how they treat the diffuse component. The isotropic model assumes that diffuse radiation is uniformly distributed across the sky dome, while the anisotropic model divides it into three components called uniform sky radiation, circumsolar radiation, and radiation from the horizon. There have been several regional studies comparing these models for determining optimum PV module tilt angle and orientation for global irradiance [34], [35], [36], [37], [38]. There have been similar modeling approaches adapted for the

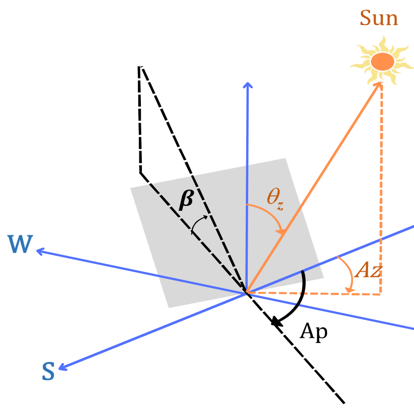

Fig. 1. Schematic representation of module tilt angle (β), solar azimuth (Az), module azimuth (Ap), and solar zenith (q_z). The gray shaded area represents the PV module.

UV radiation estimation on tilted surfaces for skin cancer and water treatment studies [39], [40], [41], [42], [43], [44], [45]. Serrano et al. [41] evaluated the UV Index (UVI) for vertical plane and 40° tilted surfaces and found that the Perez model performed best for the vertical surface; however, all the models in the study (Perez, Isotropic, Gueymard, and Muneer) show up to 17%–32% bias when validated against observations. Similarly, a study evaluated ten models for estimating the diffuse component of the UV radiation and concluded the RAU3 model performed best (with 6.1% of relative root-mean-square error) when validated against ground observations for Badajoz, Spain [39]. A recent study used an isotropic sky model approach to estimate the UV radiation on a tilted plane for solar water treatment in Chile [46]. In their study, they highlight that their modeling approach does not consider atmospheric conditions, local weather patterns, and the azimuth of the surface. There has been abundant literature that show the importance of atmospheric conditions and local climate in PV energy generation, module lifetime, and degradation mechanisms [4], [47], [48], [49], [50], [51], [52], [53]. The orientation of PV systems plays a significant role in the incident radiation on the module and its temperature, which are the two most important factors influencing degradation rates [4]. In this context, we need a more robust UV modeling approach that takes into consideration the sky dome, the influence of the atmospheric conditions, and the module azimuth.

The main objective of this study is to model incident UV radiation for both fixed-tilt and single-axis tracking (SAT) PV systems on a global scale. The novelty of this work lies in its detailed, system-specific assessment of UV exposure, which has not been comprehensively analyzed for different PV mounting configurations on a global scale. Our approach involves developing a robust UV radiation model that accounts for variations in solar position, atmospheric conditions, and system orientation. We use an anisotropic model in this study, with detailed input parameters such as the view factor of the sky, circumsolar radiation (the sky brightening near the sun), and horizon brightening (the increase in the sky radiation near the horizon), making it particularly effective under cloudy conditions. The circumsolar and horizon brightening components contribute to additional diffuse radiation on the modules, affecting the optical and thermal stress of the modules. Over time, this can accelerate material fatigue, discoloration, and delamination, particularly at the edges or around cell interconnects. Accurate modeling for these effects is therefore essential for better understanding degradation patterns and improving reliability assessments of PV systems under real-world conditions. To establish confidence in our methodology, we validate our modeled results against high-fidelity ray-tracing simulations and spectroradiometer observations to ensure the accuracy of our estimates. Once validated, this model is applied to estimate and compare the degradation rates of SAT and fixed-tilt PV systems globally. By quantifying the impact of UV exposure on modules, this study provides valuable insights into long-term performance, aiding in the design and deployment of more durable and efficient PV systems worldwide.

II. Data and Methods

A. Data

We use UV irradiance data from two Baseline Surface Radiation Network (BSRN) weather stations located in Izana, Spain, and Payerne, Switzerland, to validate our model for the horizontal surface. BSRN collects high-precision ground-based measurements of solar and thermal radiation globally to monitor Earth's energy balance. This data has been widely used for validating satellite observations, improving climate models, and supporting solar energy research. We have obtained five years of data from these stations for the period 2019–2023.

In this study, we use the atmospheric variables surface reaching downwelling radiation (GHI), air, and 2 m dew point temperature, and 10 m u (eastward wind) and v (northward wind) wind components from the European Centre for Medium Range Weather Forecasts (ECMWF) Reanalysis (ERA5) [54] dataset available at $\sim$31 km spatial resolution for modeling UV radiation on a tilted surface. We use hourly data from 2004 to 2024 to obtain the global plots.

B. Modeling Global UV Irradiance and Relative Humidity

ERA5 provides relative humidity at various pressure levels, with the lowest pressure level at 1000 hPa, which approximately corresponds to a height of 100 m. Considering that ground-mounted PV systems have heights in the range of 1.5–2.5 m, using ERA5 relative humidity for our analysis would be inaccurate. Therefore, we model surface relative humidity from saturation vapor pressure over water (using the air temperature and dew point temperature at 2 m) following the August–Roche–Magnus equation [55]. To have a consistent height for our analysis, we calculate the wind speed by translating the wind speed at 10 m to 2 m height using the power law [56], [57]. ERA5 reanalysis data provide UV irradiance covering wavelengths 200–440 nm, while the 280–380 nm range is the most important for degradation-related analysis, as used in this work. The difference in UV estimation due to overestimation of the wavelength range from reanalysis can be up to 45% higher when compared with observations [25]. This discrepancy can result in a significant difference in the estimated UV photodegradation. We model global UV radiation (wavelength <380 nm) as proposed by Wald [58]. This method has been previously used in several UV degradation modeling studies [4], [59]. UV global radiation *(*UV_g*)* is estimated based on the surface reaching downward radiation and restricted clearness index (*kt*∗) as per (1) and (2). *kt*∗ refines standard clearness index (*kt)* values by constraining extreme variations, ensuring more accurate diffuse radiation estimates particularly under clear or partly cloudy conditions where anisotropic sky behavior dominates. *Kt* is calculated as the ratio of GHI to extraterrestrial radiation on a horizontal surface.

$$\begin{aligned}\mathrm{UV}_g = \; & \left[(7.210 \; - 2.365 \; kt^*) \times 10^{-2} \times \; \mathrm{GHI}\right] \\ & + \left[(1.897 - 0.860 \; kt^*) \times 10^{-3} \times \; \mathrm{GHI}\right] \qquad (1)\end{aligned}$$

$$kt^* = \max\left(0.1, \min\left(kt, 0.7\right)\right). \qquad (2)$$

C. Modeling UV Irradiance on a Tilted Surface

The total or global irradiance comprises direct and diffuse radiation components across all wavelengths when accounting for the solar position at any given location. The UV irradiance incident on a tilted PV module is composed of direct *(*$\mathrm{UV}_{\mathrm{direct}\,,t}$*)*, diffuse *(*$\mathrm{UV}_{\mathrm{diffuse}\,,t}$*)*, and reflected UV *(*$\mathrm{UV}_{\mathrm{reflected}\,,t}$*)* from the top of the module. These components depend on the PV module's tilt (β), solar azimuth (Az), module azimuth (Ap), and solar zenith ($\mathrm{q_z}$). Fig. 1 shows the schematic of the different angles used in this study.

$$\mathrm{UV}_{g,t} = \; \mathrm{UV}_{\mathrm{direct},t} + \; \mathrm{UV}_{\mathrm{diffuse},t} + \; \mathrm{UV}_{\mathrm{reflected},t}. \qquad (3)$$

The reflected component of UV is dependent on the albedo of the ground and can be obtained using (4), assuming the reflectivity from the surface is isotropic. The direct component of UV irradiance is dependent on the diffuse fraction, the tilt of the plane, and global UV irradiance adapted from the DISC model [60]. The diffuse component of UV irradiance, estimated based on Klucher [61], is dependent on the module tilt, azimuth, and angle of incidence (aoi) projection. The aoi refers to the angle formed between the perpendicular to the PV module surface and the direction of the incoming radiation. In this study, $\mathrm{UV}_{\mathrm{direct}\,,t}$ *is modeled with simplification based on the elevation and tilt angle* (cos($\beta + \gamma$)) and can be replaced by aoi for estimating tilted component of UV radiation. This simplification can introduce very minimal bias

$$\mathrm{UV}_{\mathrm{reflected},t} = \frac{1}{2} \times albedo \times \mathrm{UV}_g \times (1 - \cos\beta) \qquad (4)$$

$$\begin{aligned}\mathrm{UV}_{\mathrm{direct},t} = & \frac{1}{2} \; \times \mathrm{UV}_g \times (1 - \text{diffuse fraction}) \\ & \times \cos\left(\beta + \gamma\right) \qquad (5)\end{aligned}$$

$$\begin{aligned}\mathrm{UV}_{\mathrm{diffuse},t} = \; & \mathrm{UV}_g \times \text{diffuse fraction} \times \text{term 1} \times \text{term2} \\ & \times \text{term3} \qquad (6)\end{aligned}$$

where γ is the elevation angle; term1, term2, and term3 can be estimated as follows:.

$$\text{term1} \; = \; 0.5 \; \times \; (1 \; + \cos\left(\beta\right)) \qquad (7)$$

$$\text{term2} \; = \; 1 \; + \; F \times \sin\left(\left(\frac{\beta}{2}\right)^3\right) \qquad (8)$$

$$\text{term3} \; = \; 1 \; + \; F \; \times \left(\max\left(\text{aoi}, 0\right)\right)^2 \; \times \sin({\theta_z}^3) \qquad (9)$$

$$\begin{aligned}\text{aoi} \; = & \left(\cos\left(\beta\right) \; \times \cos\left(\theta_z\right)\right) + \; \left(\sin\left(\beta\right) \times \sin\left(\theta_z\right)\right. \\ & \left. \times \cos\left(\text{Az} - \text{Ap}\right)\right) \qquad (10)\end{aligned}$$

The diffuse fraction is estimated by

$$\text{diffuse fraction} = \begin{cases} 1 - a \times Kuv, Kuv \leq 0.22 \\ b - c \times Kuv + d \times Kuv^2 - e \times Kuv^3 \\ \quad + f \times Kuv^4, 0.22 < Kuv \leq 0.8 \\ 0.165, Kuv > 0.8 \end{cases} \qquad (11)$$

where *a, b, c, d, e,* and *f* are 0.09, 0.9511, 0.1604, 4.388, 16.638, and 12.336, respectively, where *a* is the scaling factor that modifies diffuse fractions at clear-sky conditions, while *b*, *c*, *d*, *e*, and *f* are polynomial coefficients that refine the diffuse fraction for higher values of *Kuv*, accounting for effects such as Rayleigh scattering, aerosol interactions, and cloud cover. *Kuv* is the ratio of the global UV radiation and top-of-the-atmosphere UV radiation ($\mathrm{UV_{TOA}}$). The top of the atmosphere UV radiation can be estimated from the eccentricity of the Earth (*eccentricity*), solar constant for UV (*S*), and the zenith angle.

$$Kuv \; = \; \frac{\mathrm{UV}_{\mathrm{global}_{\mathrm{horizontal}}}}{\mathrm{UV_{TOA}}} \qquad (12)$$

$$\mathrm{UV_{TOA}} \; = \; S \times \text{eccentricity} \times \; \cos\left(\theta_z\right). \qquad (13)$$

D. Modeling UV Photodegradation

In this study, we show the application of our UV dose calculation method by adapting the module level photodegradation (called UV photodegradation here) framework by Kaaya et al. [23]. It should be noted that this model does not include UVID, that is recently been reported for TOPCon and HJT, and is expected to be a lot more severe. UV-induced photodegradation is dependent on module temperature (T_m, in Kelvin), relative humidity on the module surface (rh_{eff}, in %), and UV radiation on a tilted surface ($UV_{g,t}$), which can be estimated as follows:

$$\begin{aligned}\deg \; = & \; A_p \; \times {UV_{g,t}}^X \; \times \left(1 + rh_{\mathrm{eff}}\right)^X \\ & \times \exp\left(-\frac{E_p}{K_B \; \times \; T_m}\right) \qquad (14)\end{aligned}$$

where the activation energy required for UV photodegradation is represented by $\mathrm{E_P}$ (0.45 eV), and the impact of UV radiation on PV degradation is denoted by *X* (taken as 0.63). A_P (taken as 71.83) is the pre-exponential constant, and $\mathrm{k_B}$ is the Boltzmann constant (8.62 × 10−5eV/K) in the equation. We use the Faiman temperature model [62] to estimate the module temperature as follows:

$$T_m \; = \; T_a + \frac{\text{POA}}{U_0 + U_1 \times \text{wind speed}} \qquad (15)$$

where T_a is the air temperature (°C), and U_o and U_1 are constant heat transfer components and convective heat transfer

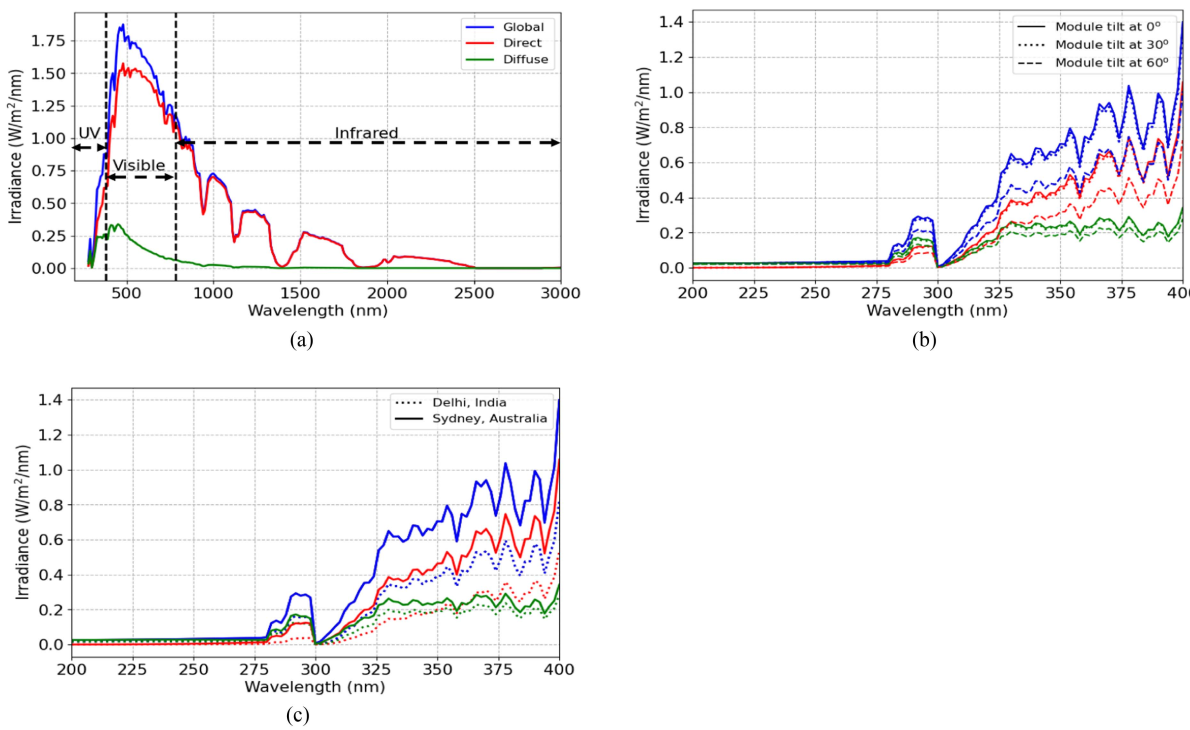

Fig. 2. (a) Spectral irradiance for Sydney, Australia, showing the UV, infrared, and visible parts of the spectrum. (b) UV spectral irradiance for Sydney, Australia, showing different irradiance components for a module with tilt angles of 0° (shown in bold line), 30° (shown in dotted line), and 60° (shown in dashed line). (c) UV spectral irradiance for Sydney, Australia (shown in bold line) and New Delhi, India (shown in dotted line) showing different irradiance components for modules with a tilt angle of 0°. Global, direct, and diffuse irradiance are shown in blue, red, and green colours, respectively, for all the plots. All the plots have been obtained using the solar spectrum calculator in PV Lighthouse software for 12th January 2024.

components, respectively (considered as 25 W/m^2 °C and 6.8 [W/m^2 /(m/s) °C], respectively). POA (W/m^2) is the incident irradiance on the plane of the module. It should be noted that the activation energy used in this equation is for monocrystalline silicon modules obtained from the previous study [23]. The degradation rate for different technologies may vary based on their activation energy.

E. Model Validation

We estimate the mean bias error and the mean bias percentage error to validate our modeling results with observations.

$$\text{Mean Bias Error } = \frac{1}{n}\sum_{i=1}^{n}(\text{Model}_i - \text{Observation}_i) \tag{16}$$

$$\text{Mean Bias Percentage Error}$$
$$= 100 \times \frac{1}{n}\sum_{i=1}^{n}\frac{\text{Model}_i - \text{Observation}_i}{\text{Observation}_i}. \tag{17}$$

III. Result and Discussion

A. UV Irradiance Spectrum

Ground reaching solar radiation consists of both direct and diffuse components and comprises three main spectral regions: UV (3% –5%), visible light (42% –43%), and infrared (52% –55%) [63]. Fig. 2(a) shows the solar spectrum for Sydney, Australia, obtained using ray tracing for radiation incident on a horizontal plane. Using ray tracing, we can clearly identify the difference in UV radiation in the spectrum for different tilt angles of the solar panels facing the equator [see Fig. 2(b)]. This highlights that net UV radiation incident on a module is dependent on its tilt angle at any given time. As a result, we can expect similar modules with different mounting, orientation, and technology to have different UV photodegradation rates. Furthermore, modules with similar mounting, orientation, and technology can exhibit significantly different degradation rates due to the geographical variability of the UV spectrum [see Fig. 2(c)]. For example, the total UV radiation incident horizontally is almost 1.4× higher for Sydney (66.9 W/m^2) than New Delhi (49.2 W/m^2). This difference is due to variations in altitude, ozone, atmospheric constituents, and other factors. This highlights that similar modules located at different geographical locations will experience UV degradation at varying rates. Based on the ray-tracing case studies in Fig. 2, it is essential to analyze UV irradiance globally for both fixed-tilt and SAT systems. However, using ray-tracing algorithms for larger datasets (such as those with 20 years or more of available hourly data) worldwide becomes computationally expensive.

We validate our UV irradiance model over the horizontal surface using weather station data recorded at Payerne, Switzerland, and Izaña, Spain (wavelength range 280–400 nm). Modeled UV irradiance from ERA5 is compared with the station observations for the time period 2019–2023 (see Table I). Model validation results show a minimum bias for both locations. Payerene has

TABLE I
UV-IRRADIANCE MODEL VALIDATION FOR HORIZONTAL SURFACE FOR TWO BSRN SITES LOCATED IN IZANA, SPAIN, AND PAYERNE, SWITZERLAND

Location	Latitude, Longitude	Köppen climate classification	Mean Bias Error
Izana, Spain	28.3094 ° N, 16.4993 ° W	humid continental climate (Dfb)	-3.87 W/m^2 (-4.08%)
Payerne, Switzerland	46.8123 ° N, 6.9422 ° E	temperate dry summer climate (Cbs)	2.22 W/m^2 (4.28%)

TABLE II
COMPARISON OF GLOBAL UV RADIATION FOR DIFFERENT TILT ANGLES OBTAINED USING RAY TRACING AND THE EMPIRICAL METHOD FOR TWO LOCATIONS ACROSS THE WORLD

Location	Latitude/ Longitude	Köppen climate classification	Mean Bias Error	
			module tilt = 30º	module tilt = 60º
Sydney, Australia	33.87 S, 151.21 E	humid continental climate (Dfb)	0.85 W/m^2 (2.07%)	-1.16 W/m^2 (-3.24%)
New Delhi, India	28.61 N, 77.20 E	temperate dry summer climate (Cbs)	-0.11 W/m^2 (-0.27 %)	-0.89 W/m^2 (-2.46%)

a positive bias (2.18 W/m^2), while we observe a negative bias for Izana (-3.96 W/m^2). A previous study by García et al. [64] highlighted that surface albedo at Izaña varies throughout the day due to its mountainous topography, as well as aerosol and cloud variability. This variability can contribute to an approximate 10% discrepancy between measured and modeled global UV radiation. It should be noted that UV radiation measurements on tilted surfaces and SAT systems are scarcely available globally, highlighting a significant gap in current observational datasets.

We compare our model output values for tilted UV radiation to UV radiometer measurements at Platforma Solar de Almería (PSA), Spain (at 37^0 tilt angle), from a previous study [42] to validate our model for tilted surface. On comparing tilted UV radiation obtained by our proposed method with UV radiometer observations for PSA, Spain, for similar time periods 2007–2010, we obtain a similar seasonal trend of UV radiation for tilted surface with a positive bias of 1.32% or 3.4Wh/m^2. The positive bias is due to the radiometer measurements being recorded only for a part of the UV spectrum (315–378 nm).

We also compare global UV irradiance over a tilted module obtained by raytracing using SunSolve from PV Lighthouse [65] and our method stated above in (3) (see Table II). The ray-tracing framework estimates UV radiation on the tilted surface of the tracking systems by explicitly resolving the angular distribution of broadband and UV irradiance on the module surface, providing a physically consistent benchmark for the subsequent ERA5-based large-scale modeling. The SunSolve raytracing algorithm has been rigorously validated for different PV technologies and orientation and has been shown to deliver accurate results with minimal bias [66], [67], [68]. The comparison is made for tilt angles of 30^0 and 60° for the locations Sydney and New Delhi for the year 2024 for clear-sky conditions. The raytracing algorithm in SunSolve computes the spectrum over clear-sky conditions and airmass 1.5 (AM1.5). Hence, the comparison is done using ERA5 clear sky radiation and noon when the sun is directly overhead for the year 2024. The comparison reveals minimal differences in the tilted global UV radiation between computationally expensive ray tracing and our proposed method, demonstrating the method's wide applicability for global studies with larger datasets. It should be noted that previous literature has found a region-dependent bias in ERA5 GHI values [48], [69], [70], which can result in biases observed.

It should be noted that UV radiation for global health studies is commonly measured and monitored using metrics such as UVI or UV intensity. These metrics apply a wavelength-dependent weighting factor to different wavelengths based on their varying impacts on human health (e.g., erythemal response). This weighting complicates the direct validation of our model with standardized ground measurements for tilted surfaces, which typically report weighted rather than absolute spectral irradiance values.

B. UV Radiation on Fixed Tilt and SAT Systems

We use the proposed method to calculate the global mean UV radiation for fixed tilt and solar array tracker (SAT) systems over the period 2004–2024. Fig. 3(a) and (b) shows the spatial variability of global UV radiation (temporally averaged over 20-year period, and UV dose [see Fig. 3(c) and (d)] for fixed tilt and SAT systems. We have modeled the tilt equivalent to the value of the latitude for each grid point (for fixed tilt) and azimuth as their direction to the equator [71], [72] (for both SAT and fixed tilt). UV dose is obtained by considering sunshine hours during the day. Note that these UV dose values are not weighted over wavelength as commonly applicable in skin cancer studies. This is because UV photodegradation depends on the entire UV spectrum, rather than specific wavelengths.

Results show higher values of UV radiation for SAT [see Fig. 3(b)], globally up to 1.5× (or ∼15 W/m^2) higher in comparison to the fixed-tilt system [see Fig. 3(a)]. Arid regions record highest tilted UV radiation for both systems with the highest values near Atacama desert (coordinates 24.5°S, 69.25°W) (up to 170 kWh/m^{2}year on SATs and ∼125 kWh/m^{2}year on fixed tilt systems), the Saharan desert (coordinates 23.41°N, 25.66°W) (up to 160 kWh/m^{2}year on SATs and up to 120 kWh/m^{2}year on fixed tilt systems), middle east (∼150 kWh/m^{2}year on SATs and ∼110 kWh/m^{2}year on fixed tilt systems), and northern Australia (up to 155 kWh/m^{2}year on SATs and up to 105 W/m^2 on fixed tilt systems). This difference in UV radiation between the two systems is due to the varying plane of array irradiance on each system. SAT systems can receive up to 20% higher irradiance annually than a fixed tilt system, depending on the region of installation. It should be noted that IEC 61215 UV test exposes modules to just 15 kWh/m^2, which is far below the cumulative UV dose expected in high-irradiance regions (see Fig. 3). More rigorous protocols such as IEC TS 62788-7-2 (up to 100 kWh/m^2 for material testing), NREL's UV-enhanced aging procedures (>60–80 kWh/m^2 to replicate harsher climates in combination

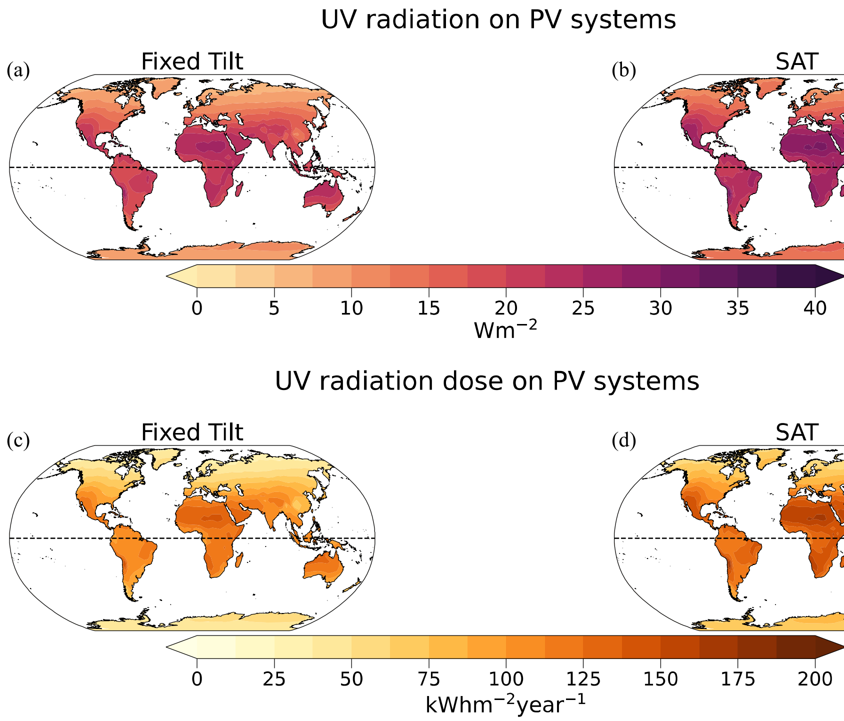

Fig. 3. UV radiation for (a) fixed tilt and (b) SAT systems for 2004–2024. Panels (c) and (d) show the UV radiation dose on the fixed tilt and SAT system, respectively. The black dashed line shows the equator.

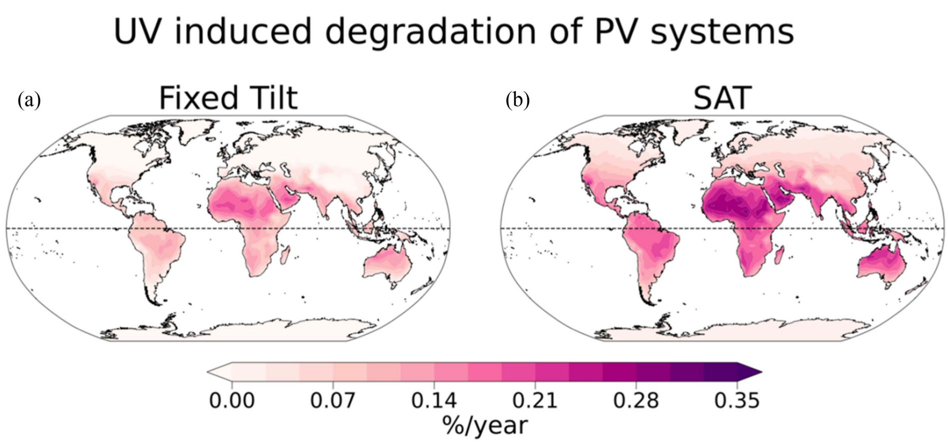

Fig. 4. Annual mean UV photodegradation rate for (a) fixed tilt and (b) SAT systems using ERA5 reanalysis data for 2004–2024. The black dashed line shows the equator.

with damp heat tests) [22], [73], and ASTM G154/G155 [74] still fall short of replicating the real 25–30 year field exposure. These results highlight the need for region-specific and dose-realistic testing to capture long-term UV degradation more accurately.

C. Worldwide UV Photodegradation for Fixed Tilt and SAT Systems

Module temperature, moisture, and UV radiation on the module drive the UV photodegradation mechanism, also referred to as photodegradation. It can initiate several module failures, such as encapsulant discoloration, delamination, and ribbon discoloration, among others, and cause early aging of the modules. In this research, we show the applicability of our proposed UV radiation model in estimating UV photodegradation rates. The degradation rates are obtained using an empirical kinetic model that accounts for the three climate stressors (UV radiation, temperature, and effective relative humidity) [23]. This model has been validated with both indoor experimental data (mean bias 0.19%) and outdoor field observations (mean bias 2.34%), ensuring confidence in its reliability and robustness. This model does not estimate degradation from any specific failure mechanism; rather, it provides a generic, module-specific degradation rate associated with UV radiation exposure on the module surface.

Annual mean UV photodegradation rate for fixed tilt and SAT PV systems is shown in Fig. 4. We observe a higher degradation rate for the modules installed in the tropical regions and regions with arid climates. The spatial distribution of the degradation rates for both systems [see Fig. 4(a) and (b)] is similar to the spatial distribution of UV radiation and dose [see Fig. 3(a)–(d)]. The tropical regions experience higher temperature, radiation, and humidity, while arid regions have higher temperature and radiation. Saharan regions and the Middle East record the highest simulated degradation rate (up to 0.25% /year and 0.35% /year for fixed tilt and SAT systems, respectively). Northern Australia records degradation up to 0.15% /year - 0.2% /year, depending on the system type. Furthermore, UV photodegradation can be up to 15% higher for SATs [see Fig. 4(b)] than fixed tilt systems, depending on the location where they are installed. Our results show a similar spatial distribution for the induced degradation rate with previous studies [4], [25], but significantly higher degradation rates for the regions close to the equator. Although an annual UV photodegradation rate of 0.35% /year may appear modest, it results in a cumulative loss of approximately 5% over a 20-year operational lifetime.

Previous studies have highlighted that [25] UV photodegradation can serve as a catalyst for secondary failure modes, such as encapsulant discoloration, delamination, and corrosion, among others, further accelerating performance loss [75], [76]. Prolonged exposure to UV radiation and elevated temperatures can trigger photocatalytic reactions, resulting in surface degradation. UV radiation, in particular, causes discoloration of the module, which may lead to localized heat accumulation. This heat trapping can subsequently induce delamination of the encapsulant due to reduced adhesive strength [77]. It is important to note, however, that distinguishing the individual effects of UV radiation and moisture ingress on encapsulant delamination remains a significant challenge [12].

These findings highlight the critical importance of accounting for climate-induced degradation mechanisms in system design, including site selection, mounting configuration, and the use of materials with enhanced resistance to UV exposure and coupled thermal-hydro stressors. Modern module technologies, such as TOPCon, HJT, and PERC, have antireflective coatings, and their optical performance and UV absorption can vary significantly with wavelength. Therefore, it is recommended to develop a better model in the future that accounts for the spectral and optical response of these modern technologies.

IV. Conclusion

Accurate estimation and modeling of UV radiation on tilted surfaces is essential for precise UV photodegradation modeling. In this study, we demonstrate a robust method to calculate UV radiation on tilted surfaces that uses solar position, atmospheric conditions, and system orientation. The method can be universally applied for both fixed tilt and tracking systems. On comparing our method with ray-tracing simulations and radiometer observations, we observe a minimum bias ($<$1.6%), therefore establishing confidence in our approach. We observe higher UV radiation values near the arid and semi-arid regions for both the systems, with SATs recording higher UV radiation than the fixed-tilt systems. On modeling UV photodegradation on tilted surfaces, we find higher degradation rates in the regions with tropical, arid, and semi-arid conditions. This is due to higher temperature, humidity, and irradiation in these areas. Even though regions with arid and semi-arid climate types have lower levels of humidity, they receive higher insolation due to clearer skies and record higher temperatures, which contribute to higher UV photodegradation.

Our results highlight that modules with similar technology and orientation can still exhibit region-specific degradation. This is due to the influence of local weather and climate when exposed to outdoor conditions. This underscores the need for climate-specific indoor testing and accelerated tests for reliability and better lifetime predictions. Notably, UV photodegradation alone can account for nearly a quarter of the total annual degradation in monocrystalline silicon modules in regions with high UV dose, potentially reducing system lifetime by 7–10 years. This results in higher maintenance costs and thereby negatively impacts the levelized cost of energy generation. Therefore, this work will be highly beneficial in accurate UV photodegradation modeling, lifetime predictions, technology, and material selection globally.

Acknowledgment

The authors would like to thank the World Radiation Monitoring Center (WRMC) and BSRN for collecting, calibrating, validating, and sharing the data freely on https://bsrn.awi.de. The authors also thank ECMWF climate data store (CDS) for hosting and sharing ERA5 reanalysis data (https://cds.climate.copernicus.eu). All the computation was done on the Australian National Supercomputing Infrastructure (NCI) GADI. Responsibility for the views, information, or advice expressed herein is not accepted by the Australian Government.

Data availability: This work is based on the open-source data freely available from the BSRN (https://bsrn.awi.de) and ECMWF ERA5 reanalysis data (https://cds.climate.copernicus.eu).

References

[1] "IRENA (2024). World Energy Transitions Outlook 2024: 1.5°C pathway. Accessed: Nov. 23, 2025. [Online]. Available: https://www.irena.org/-/media/Files/IRENA/Agency/Publication/2024/Nov/IRENA_World_energy_transitions_outlook_2024.pdf

[2] "IEA (2025). Renewables 2025, IEA, Paris. Accessed: Nov. 23, 2025. [Online]. Available: https://www.iea.org/reports/renewables-2025, Licence: CC BY 4.0.

[3] J. Kim et al., "A review of the degradation of photovoltaic modules for life expectancy," *Energies (Basel)*, vol. 14, no. 14, Jul. 2021, Art. no. 4278, doi: 10.3390/en14144278.

[4] S. Poddar et al., "Accelerated degradation of photovoltaic modules under a future warmer climate," *Prog. Photovolt., Res. Appl.*, vol. 32, no. 7, pp. 456–467, 2023.

[5] L. Dunn, M. Gostein, and B. Stueve, "Literature review of the effects of UV exposure on PV modules," *NREL PV module reliability workshop*, 2013, pp. 1–19.

[6] P. Y. Yuen, S. L. Moffitt, F. D. Novoa, L. T. Schelhas, and R. H. Dauskardt, "Tearing and reliability of photovoltaic module backsheets," *Prog. Photovolt., Res. Appl.*, vol. 27, no. 8, pp. 693–705, 2019, doi: 10.1002/pip.3144.

[7] H. Gopalakrishna, P. Arularasu, K. Dolia, A. Sinha, and G. Tamizhmani, "Characterization of encapsulant degradation in accelerated UV stressed mini-modules with UV-cut and UV-pass EVA," in *Proc. IEEE 46th Photovolt. Spec. Conf.*, 2019, pp. 1961–1964, doi: 10.1109/PVSC40753.2019.8980897.

[8] D. C. Miller et al., "Degradation in PV encapsulation transmittance: An interlaboratory study towards a climate-specific test," in *Proc. IEEE 42nd Photovolt. Spec. Conf.*, 2015, pp. 1–6, doi: 10.1109/PVSC.2015.7355607.

[9] O. Boucher et al., "Clouds and aerosols," in *Climate Change 2013: The Physical Science Basis. Contribution of Working Group I to the Fifth Assessment Report of the Intergovernmental Panel On Climate Change*, T. F. Stocker Eds., Cambridge, U.K.: Cambridge University Press, 2013, pp. 571–657, doi: 10.1017/CBO9781107415324.016.

[10] A. Sinha et al., "Prediction of climate-specific degradation rate for photovoltaic encapsulant discoloration," *IEEE J. Photovolt.*, vol. 10, no. 4, pp. 1093–1101, Jul. 2020, doi: 10.1109/JPHOTOV.2020.2989182.

[11] S. Uličná et al., "PV encapsulant formulations and stress test conditions influence dominant degradation mechanisms," *Sol. Energy Mater. Sol. Cells*, vol. 255, 2023, Art. no. 112319, doi: 10.1016/j.solmat.2023.112319.

[12] B. Bora, S. Rai, A. Dhar, and C. Banerjee, "Effect of UV irradiation on PV modules and their simulation in newly designed site-specific accelerated ageing tests," *Sol. Energy*, vol. 253, pp. 309–320, Mar. 2023, doi: 10.1016/j.solener.2023.02.042.

[13] C. R. Osterwald, J. Pruett, and T. Moriarty, "Crystalline silicon short-circuit current degradation study: Initial results," 2005. [Online]. Available: http://www.osti.gov/bridge

[14] "Kiwa PVEL PV module reliability scorecard," 2025. Accessed: Nov. 23, 2025. [Online]. Available: https://scorecard.pvel.com/

[15] S. Razzaq et al., "Enhancing UV light stability in commercial silicon HJT solar cells and modules," *Sol. Energy*, vol. 298, Sep. 2025, Art. no. 113735, doi: 10.1016/J.SOLENER.2025.113735.

[16] L. Yang et al., "Insights into mechanism of UV-induced degradation in silicon heterojunction solar cells," *Sol. Energy Mater. Sol. Cells*, vol. 275, Sep. 2024, Art. no. 113022, doi: 10.1016/J.SOLMAT.2024.113022.

[17] R. Witteck et al., "UV radiation hardness of photovoltaic modules featuring crystalline Si solar cells with AlO/p+-type Si and SiN/n+-type Si interfaces," *Physica Status Solidi–Rapid Res. Lett.*, vol. 11, no. 8, 2017, Art. no. 1700178, doi: 10.1002/pssr.201700178.

[18] F. T. Thome et al., "UV-induced degradation of industrial PERC, TOPCon, and HJT solar cells: The next big reliability challenge?," *Sol. RRL*, vol. 8, no. 23, 2024, Art. no. 2400628, doi: 10.1002/solr.202400628.

[19] A. Sinha et al., "UV-induced degradation of high-efficiency silicon PV modules with different cell architectures," *Prog. Photovolt., Res. Appl.*, vol. 31, no. 1, pp. 36–51, 2023, doi: 10.1002/pip.3606.

[20] W. Gu, T. Ma, S. Ahmed, Y. Zhang, and J. Peng, "A comprehensive review and outlook of bifacial photovoltaic (bPV) technology," *Energy Convers. Manage.*, vol. 223, 2020, Art. no. 113283, doi: 10.1016/j.enconman.2020.113283.

[21] M. P. Maniscalco, S. Longo, G. Miccichè, M. Cellura, and M. Ferraro, "A critical review of the environmental performance of bifacial photovoltaic panels," *Energies*, vol. 17, no. 1, 2024, Art. no. 226, doi: 10.3390/en17010226.

[22] J. Wohlgemuth and S. Kurtz, "Photovoltaic module qualification plus testing," in *Proc. IEEE 40th Photovolt. Spec. Conf.*, 2014, pp. 3589–3594, doi: 10.1109/PVSC.2014.6924883.

[23] I. Kaaya, M. Koehl, A. P. Mehilli, S. De Cardona Mariano, and K. A. Weiss, "Modeling outdoor service lifetime prediction of PV modules: Effects of combined climatic stressors on PV module power degradation," *IEEE J. Photovolt.*, vol. 9, no. 4, pp. 1105–1112, Jul. 2019, doi: 10.1109/JPHOTOV.2019.2916197.

[24] S. Lindig, I. Kaaya, K. A. Weis, D. Moser, and M. Topic, "Review of statistical and analytical degradation models for photovoltaic modules and systems as well as related improvements," *IEEE J. Photovolt.*, vol. 8, no. 6, pp. 1773–1786, Nov. 2018, doi: 10.1109/JPHOTOV.2018.2870532.

[25] J. Ascencio-Vásquez, I. Kaaya, K. Brecl, K. A. Weiss, and M. Topič, "Global climate data processing and mapping of degradation mechanisms and degradation rates of PV modules," *Energies (Basel)*, vol. 12, no. 24, pp. 1–16, 2019, doi: 10.3390/en12244749.

[26] C. Gueymard, "An anisotropic solar irradiance model for tilted surfaces and its comparison with selected engineering algorithms," *Sol. Energy*, vol. 38, no. 5, pp. 367–386, Jan. 1987, doi: 10.1016/0038-092X(87)90009-0.

[27] Y. F. Nassar, A. A. Hafez, and S. Y. Alsadi, "Multi-factorial comparison for 24 distinct transposition models for inclined surface solar irradiance computation in the state of Palestine: A case study," *Front. Energy Res.*, vol. 7, Feb. 2020, Art. no. 511014, doi: 10.3389/FENRG.2019.00163/BIBTEX.

[28] A. Buonomano et al., "Prediction of global solar irradiance on parallel rows of tilted surfaces including the effect of direct and anisotropic diffuse shading," *Energies*, vol. 17, no. 14, Jul. 2024, Art. no. 3444, doi: 10.3390/EN17143444.

[29] M. Tamoor, A. R. Bhatti, M. Farhan, A. Rasool, and A. Sherefa, "Optimizing tilt angle of PV modules for different locations using isotropic and anisotropic models to maximize power output," *Sci. Rep.*, vol. 14, no. 1, Dec. 2024, Art. no. 30197, doi: 10.1038/s41598-024-81826-9.

[30] M. J. Mayer and G. Gróf, "Extensive comparison of physical models for photovoltaic power forecasting," *Appl. Energy*, vol. 283, Feb. 2021, Art. no. 116239, doi: 10.1016/J.APENERGY.2020.116239.

[31] A. J. and W. A. Beckman. Duffie, *Solar Engineering of Thermal Processes*. Hoboken, NJ, USA: Wiley, 2013.

[32] T. Muneer, *Sol. Radiat. and Daylight Models*, 2nd ed. Evanston, IL, USA: Routledge, 2004.

[33] B. Liu and R. Jordan, "Daily insolation on surfaces tilted towards equator," *ASHRAE J. (United States)*, vol. 10, pp. 53–59, Oct. 1961.

[34] T. O. Kaddoura, M. A. M. Ramli, and Y. A. Al-Turki, "On the estimation of the optimum tilt angle of PV panel in Saudi Arabia," *Renewable Sustain. Energy Rev.*, vol. 65, pp. 626–634, Nov. 2016, doi: 10.1016/J.RSER.2016.07.032.

[35] M. S. Khan, M. A. M. Ramli, H. F. Sindi, T. Hidayat, and H. R. E. H. Bouchekara, "Estimation of solar radiation on a PV panel surface with an optimal tilt angle using electric charged particles optimization," *Electronics*, vol. 11, no. 13, Jun. 2022, Art. no. 2056, doi: 10.3390/ELECTRONICS11132056.

[36] A. Barbón, C. Bayón-Cueli, L. Bayón, and C. Rodríguez-Suanzes, "Analysis of the tilt and azimuth angles of photovoltaic systems in non-ideal positions for urban applications," *Appl. Energy*, vol. 305, Jan. 2022, Art. no. 117802, doi: 10.1016/J.APENERGY.2021.117802.

[37] Q. Hassan et al., "Experimental investigation for the estimation of the intensity of solar irradiance on oblique surfaces by means of various models," *Energy Harvesting Syst.*, vol. 9, no. 2, pp. 227–237, Nov. 2022, doi: 10.1515/EHS-2021-0087/ASSET/GRAPHIC/J_EHS-2021-0087_FIG_020.JPG.

[38] S. A. M. Maleki, H. Hizam, and C. Gomes, "Estimation of hourly, daily and monthly global solar radiation on inclined surfaces: Models re-visited," *Energies*, vol. 10, no. 1, Jan. 2017, Art. no. 134, doi: 10.3390/EN10010134.

[39] G. Sanchez, A. Serrano, and M. L. Cancillo, "Modeling the erythemal surface diffuse irradiance fraction for Badajoz, Spain," *Atmos. Chem. Phys.*, vol. 17, no. 20, pp. 12697–12708, Oct. 2017, doi: 10.5194/acp-17-12697-2017.

[40] G. Sanchez, A. Serrano, and M. L. Cancillo, "Modeling erythemal ultraviolet diffuse fraction,," *Atmos. Chem. Phys.*, vol. 17, pp. 12697–12708, doi: 10.5194/acp-2017-524.

[41] D. Serrano, M. J. Marín, M. P. Utrillas, F. Tena, and J. A. Martínez-Lozano, "Modelling of the UV Index on vertical and 40° tilted planes for different orientations," *Photochem. Photobiol. Sci.*, vol. 11, no. 2, pp. 333–344, 2012, doi: 10.1039/c1pp05211j.

[42] L. C. Navntoft, P. Fernandez-Ibañez, and F. Garreta, "UV solar radiation on a tilted and horizontal plane: Analysis and comparison of 4years of measurements," *Sol. Energy*, vol. 86, no. 1, pp. 307–318, 2012, doi: 10.1016/j.solener.2011.10.004.

[43] L. González-Rodríguez et al., "Spatio-temporal estimations of ultraviolet erythemal radiation in Central Chile," *Air Qual., Atmos. Health*, vol. 15, no. 5, pp. 837–852, May 2022, doi: 10.1007/S11869-022-01195-Y/FIGURES/7.

[44] M. Rivas et al., "Solar ultraviolet A radiation and nonmelanoma skin cancer in Arica, Chile," *J. Photochem. Photobiol. B, Biol.*, vol. 212, Nov. 2020, Art. no. 112047, doi: 10.1016/j.jphotobiol.2020.112047.

[45] L. González-Rodríguez, A. Cabrera-Reina, J. Rosas, M. Volke, and A. Marzo, "Characterization of solar-derivate ultraviolet radiation for water solar treatment applications," *Renewable Energy*, vol. 233, Oct. 2024, Art. no. 121078, doi: 10.1016/J.RENENE.2024.121078.

[46] L. González-Rodríguez et al., "Tilted solar UV radiation estimation and its role in advanced solar water treatment systems," *Sol. Energy*, vol. 295, Jul. 2025, Art. no. 113521, doi: 10.1016/J.SOLENER.2025.113521.

[47] S. Poddar, M. Kay, and J. Boland, "A standardized sky condition classification method for multiple timescales and its applications in the solar industry," *Energies*, vol. 17, no. 18, 2024, Art. no. 4616, doi: 10.3390/en17184616.

[48] S. Poddar, J. P. Evans, M. Kay, A. Prasad, and S. Bremner, "Estimation of future changes in photovoltaic potential in Australia due to climate change," *Environ. Res. Lett.*, vol. 16, no. 11, Nov. 2021, Art. no. 114034, doi: 10.1088/1748-9326/ac2a64.

[49] S. Poddar, P. J. Evans, M. Kay, A. Prasad, and S. Bremner, "Assessing Australia's future solar power ramps with climate projections," *Sci. Rep.*, vol. 13, 2023, Art. no. 11503.

[50] S. Poddar, M. Kay, A. Prasad, J. P. Evans, and S. Bremner, "Changes in solar resource intermittency and reliability under Australia's future warmer climate," *Sol. Energy*, vol. 266, 2023, Art. no. 112039, doi: 10.1016/j.solener.2023.112039.

[51] J. A. Crook, L. A. Jones, P. M. Forster, and R. Crook, "Climate change impacts on future photovoltaic and concentrated solar power energy output," *Energy Environ. Sci.*, vol. 4, no. 9, pp. 3101–3109, 2011, doi: 10.1039/c1ee01495a.

[52] K. Solaun and E. Cerdá, "Climate change impacts on renewable energy generation. A review of quantitative projections," *Renewable Sustain. Energy Rev.*, vol. 116, 2019, Art. no. 109415, doi: 10.1016/j.rser.2019.109415.

[53] D. Burnett, E. Barbour, and G. P. Harrison, "The U.K. solar energy resource and the impact of climate change," *Renewable Energy*, vol. 71, pp. 333–343, 2014, doi: 10.1016/j.renene.2014.05.034.

[54] H. Hersbach et al., "The ERA5 global reanalysis," *Quart. J. Roy. Meteorol. Soc.*, vol. 146, no. 730, pp. 1999–2049, 2020, doi: 10.1002/qj.3803.

[55] O. A. Alduchov and R. E. Eskridge, "Improved magnus form approximation of saturation vapor pressure," *J. Appl. Meteorol. (1988-2005)*, vol. 35, no. 4, pp. 601–609, 1996. [Online]. Available: http://www.jstor.org/stable/26187406

[56] A. A. Prasad, R. A. Taylor, and M. Kay, "Assessment of solar and wind resource synergy in Australia," *Appl. Energy*, vol. 190, pp. 354–367, 2017, doi: 10.1016/j.apenergy.2016.12.135.

[57] U. B. Gunturu and C. A. Schlosser, "Characterization of wind power resource in the United States," *Atmos. Chem. Phys.*, vol. 12, no. 20, pp. 9687–9702, 2012, doi: 10.5194/acp-12-9687-2012.

[58] L. Wald, "A simple algorithm for the computation of the spectral distribution of solar irradiance at the surface," Mines ParisTech, 2018. [Online]. Available: https://hal-mines-paristech.archives-ouvertes.fr/hal-01693473v1/document

[59] J. Ascencio-Vásquez, K. Brecl, and M. Topič, "Methodology of Köppen-Geiger-Photovoltaic climate classification and implications to worldwide mapping of PV system performance," *Sol. Energy*, vol. 191, pp. 672–685, 2019, doi: 10.1016/j.solener.2019.08.072.

[60] E. L. Maxwell, "A quasi-physical model for converting hourly global horizontal to direct normal lnsolation," Tech. Rep. SERI/TR-215-3087, Golden, CO: Solar Energy Research Institute, 1987.

[61] T. M. Klucher, "Evaluation of models to predict insolation on tilted surfaces," *Solar Energy*, vol. 23, no. 2, pp. 111–114, 1979, doi: 10.1016/0038-092X(79)90110-5.

[62] D. Faiman, "Assessing the outdoor operating temperature of photovoltaic modules," *Prog. Photovolt.: Res. Appl.*, vol. 16, no. 4, pp. 307–315, 2008, pp. 307–315. [Online]. Available: https://doi.org/10.1002/pip.813

[63] L. Wang and J. Yu et al., "Chapter 1 - principles of photocatalysis," *S-scheme Heterojuncti Photocatalysts*, J. Yu, L. Zhang, L. Wang, and B. Zhu, Eds., in Interface Science and Technology, vol. 35, pp. 1–52, 2023. [Online]. Available: https://doi.org/10.1016/B978-0-443-18786-5.00002-0

[64] R. D. García et al., "Comparison of measured and modelled spectral UV irradiance at Izaña high mountain station: Estimation of the underlying effective albedo," *Int. J. Climatol.*, vol. 36, no. 1, pp. 377–388, Jan. 2016, doi: 10.1002/joc.4355.

[65] "PV Lighthouse, Accessed: Jun. 16, 2025. [Online]. Available: https://www.pvlighthouse.com.au/

[66] M. B. Hartenstein et al., "High-voltage monocrystalline Si photovoltaic minimodules based on poly-Si/SiOx passivating contacts for high-power laser power conversion," *Sol. Energy Mater. Sol. Cells*, vol. 255, Jun. 2023, Art. no. 112286, doi: 10.1016/J.SOLMAT.2023.112286.

[67] D. Chen et al., "24.58% total area efficiency of screen-printed, large area industrial silic on solar cells with the tunnel oxide passivated contacts (i-TOPCon) design," *Sol. Energy Mater. Sol. Cells*, vol. 206, Mar. 2020, Art. no. 110258, doi: 10.1016/J.SOLMAT.2019.110258.

[68] H. Lin et al., "Silicon heterojunction solar cells with up to 26.81% efficiency achieved by electrically optimized nanocrystalline-silicon hole contact layers," *Nature Energy*, vol. 8, no. 8, pp. 789–799, May 2023, doi: 10.1038/s41560-023-01255-2.

[69] D. Yang and J. M. Bright, "Worldwide validation of 8 satellite-derived and reanalysis solar radiation products: A preliminary evaluation and overall metrics for hourly data over 27 years," *Sol. Energy*, vol. 210, pp. 3–19, 2020, doi: 10.1016/j.solener.2020.04.016.

[70] R. Urraca, T. Huld, A. Gracia-Amillo, F. J. Martinez-de-Pison, F. Kaspar, and A. Sanz-Gar, "Evaluation of global horizontal irradiance estimates from ERA5 and COSMO-REA6 reanalyses using ground and satellite-based data," *Sol. Energy*, vol. 164, pp. 339–354, 2018, doi: 10.1016/j.solener.2018.02.059..

[71] J. Leloux, L. Narvarte, and D. Trebosc, "Review of the performance of residential PV systems in France," *Renewable Sustain. Energy Reviews*, vol. 16, no. 2, pp. 1369–1376, 2012, doi: 10.1016/j.rser.2011.10.018.

[72] N. Haghdadi, J. Copper, A. Bruce, and I. MacGill, "A method to estimate the location and orientation of distributed photovoltaic systems from their generation output data," *Renew. Energy*, vol. 108, pp. 390–400, 2017. [Online]. Available: https://doi.org/10.1016/j.renene.2017.02.080

[73] S. Kurtz et al., "Photovoltaic module qualification plus testing," 2013. Accessed: Jun. 17, 2025. [Online]. Available: www.nrel.gov/publications

[74] "ASTM G154 testing - applied technical services," Accessed: Jun. 17, 2025. [Online]. Available: https://atslab.com/standard/american-society-for-testing-and-materials/astm-g154-testing/#

[75] M. D. Kempe, "Modeling of rates of moisture ingress into photovoltaic modules," *Sol. Energy Mater. Sol. Cells*, vol. 90, no. 16, pp. 2720–2738, 2006, doi: 10.1016/j.solmat.2006.04.002.

[76] M. Köntges et al., "Review of Failures of Photovoltaic Modules," Nov. 2014.

[77] A. Omazic et al., "Relation between degradation of polymeric components in crystalline silicon PV module and climatic conditions: A literature review," *Sol. Energy Mater. Sol. Cells*, vol. 192, no. December 2018, pp. 123–133, Dec. 2019, doi: 10.1016/j.solmat.2018.12.027.